RESEARCH ARTICLE

Gas-Induced Electrical and Magnetic Modulation of Two-Dimensional Conductive Metal−Organic Framework

Zheng Meng,*[a,c] Robert M. Stolz,[a] Lygia Silva De Moraes,[b] Christopher G. Jones,[b] Aileen M. Eagleton,[a] Hosea M. Nelson,*[b] Katherine A. Mirica*[a]

Dedicated to Prof. George Whitesides on the occasion of his 85th birthday.

[a] Dr. Z. Meng, Dr. R. M. Stolz, A. M. Eagleton, Prof. Dr. K. A. Mirica
Department of Chemistry
Dartmouth College
Burke Laboratory, Hanover, NH 03755, USA.
E-mail: katherine.a.mirica@dartmouth.edu

[b] Dr. L. De Moraes, C. G. Jones, Prof. Dr. H. M. Nelson
Division of Chemistry and Chemical Engineering
California Institute of Technology
Pasadena, California 91125, USA.
E-mail: hosea@caltech.edu

[c] Dr. Z. Meng
School of Chemistry and Materials Science
University of Science and Technology of China
Hefei, Anhui 230026, P. R. China.
E-mail: zhengmeng@ustc.edu.cn

Supporting information for this article is given via a link at the end of the document.

Abstract: Controlled modulation of electronic and magnetic properties in stimuli-responsive materials provides valuable insights for the design of magnetoelectric or multiferroic devices. This paper demonstrates the modulation of electrical and magnetic properties of a semiconductive, paramagnetic metal−organic framework $Cu_3(C_6O_6)_2$ with small gaseous molecules, NH_3, H_2S, and NO. This study merges chemiresistive and magnetic tests to reveal that the MOF undergoes simultaneous changes in electrical conductance and magnetization that are uniquely modulated by each gas. The features of response, including direction, magnitude, and kinetics, are modulated by the physicochemical properties of the gaseous molecules. This study advances the design of multifunctional materials capable of undergoing simultaneous changes in electrical and magnetic properties in response to chemical stimuli.

Introduction

Materials that respond to external chemical stimuli through changes in electronic and magnetic properties hold tremendous potential for applications in switches, information storage, and sensors.[1] Among established transduction mechanisms,[2] promoting changes in transport characteristics and spin properties of solid state materials with chemical stimuli are particularly appealing for fabricating next-generation electronic switches, sensing, and information storage devices.[3] Synergistic use of changes in properties of charge and spin can afford large and reliable output signals since the changes of both the electrical and magnetic properties of materials are a function of the physical and chemical characteristics of their surroundings.[4] Despite the high promise, the simultaneous modulation of electrical and magnetic properties of the same material using a chemical stimulus is still lacking and hindered by two fundamental gaps in knowledge. *First*, the development of materials amenable for this type of application requires encoding multifunctionality into a single system, including the suitable conductivity that is feasible to monitor, the suitable spatial spin polarization capability, as well as the effective and selective guest analyte binding ability.[5] The lack of clear design rules for such encoding hinders progress in this area. *Second*, with few exceptions,[6] fundamental studies of the simultaneous electrical and magnetic response of materials upon external chemical stimuli, which are critical for understanding their operation in chemiresitive and magnetoresistive devices, remain largely unexplored.

Two-dimensional (2D) conductive metal–organic frameworks (MOFs),[7] emerging as a class of multifunctional nanomaterials, hold high potential in electrically transduced switches and sensing devices.[2, 8] The strategic choice of organic ligands interconnected with metal nodes can afford emergent features of conductivity, magnetic ordering, and porosity through the use of simple molecular precursors.[6b, 9] The constituents and pore structure in these materials can be designed to serve as effective host sites, offering an attractive way to tune the electrical conductivity[10] and magnetic properties[6b, 11] using guest

molecules. These combined features of 2D conductive MOFs make them a unique platform for the fundamental study of changes in multifunctional characteristics in response to external chemical stimuli.

This study investigates the electrical and magnetic response of a 2D semiconductive MOF $Cu_3(C_6O_6)_2$ to small gaseous molecules, namely NH_3, H_2S, and NO. We choose NH_3, H_2S, and NO as analytes because these molecules represent well-known toxic pollutants and biological signaling molecules.[12] These molecules also serve as distinct spectroscopic probes for fundamental investigations of material-analyte interactions due to their unique physical and chemical properties.[13] Using chemiresistive devices fabricated from the MOF, we observed distinct amplitude, reversibility, and kinetics of conductance modulations induced by the gases. Magnetic tests on the gas-exposed samples showed that all three gases also induced noticeable changes in the magnetization of the MOF, resulting in increased magnetic frustration. In each case, the distinct interactions of gas molecules with the MOF were related to the intrinsic physical and chemical properties of the participating species. Mechanistic studies using various spectroscopic techniques, including diffuse reflectance infrared Fourier transform spectroscopy (DRIFTS), X-ray photoelectron spectroscopy (XPS), and electron paramagnetic resonance (EPR) spectroscopy, revealed that the interaction for NH_3 was dominated by the dehydration of the MOF, H-bonding (Bronsted acid type interaction), and coordination to Cu (Lewis acid type interaction). H_2S exposure was characterized by the reduction of Cu(II) to Cu(I) and the partial deconstruction of the d-π conjugated structure of the MOF. The binding of NO resulted in a radical-type interaction with the ligand of the MOF. Our study, for the first time, provides fundamental insights into the dual effect on the electrical and magnetic response of a representative conductive MOF material to external chemical stimuli within a single material platform.

RESULTS and DISCUSSION

Material and Structure

We choose a semiconductive MOF, $Cu_3(C_6O_6)_2$, as the responsive material for investigating its electrical and magnetic response to chemical stimuli. While this material has been previously reported by a few research groups[14] and our group[15], its stimuli-responsive properties remain entirely unexplored. Our previous studies[15] have established that $Cu_3(C_6O_6)_2$ MOF possesses a 2D layered honeycomb network and O-decorated 1D channel in a diameter of ~1.1 nm with confined water guests inside (pore volume 0.065 cm^3/g) and exhibits semiconductive and paramagnetic properties with strong geometric magnetic frustration (**Figure 1a-b**). We hypothesized that the ability of the MOF to accommodate water molecules in the pores can be extended to intermolecular interactions with other analytes, that may induce perturbations to the MOF material, such as the extent of π-d orbital overlap between metal ions and ligands, spin distribution, and spin-spin interaction within the 2D layers.[16] These perturbations would be expected to alter the electrical and magnetic properties of the MOF. In addition, $Cu_3(C_6O_6)_2$ is one of a only several other[17] 2D semiconductive MOFs whose structure has been unambiguously determined by with atomic precision.[15] The reliable structural information of the host materials is critical for mechanistic interpretation, since the gas-induced physical properties can be sensitive to the structural details of the host material.[1f, 18] Despite the fact that structures of MOFs using other ligands with a larger size compared to $H_6C_6O_6$, including hexahydroxytriphenylene (HHTP) and hexahydroxytetraazanaphthotetraphene (HHTT), have been determined by single crystal analysis, their structure contains non-extended molecular coordination clusters composed of the corresponding ligands and metal ions,[17] which may complicate the interpretation of the material-gas interactions, since the coordination clusters have different types of binding sites compared to extended framework portion in the materials.[13b] Additionally, we reasoned that the concise and compact structural feature of $Cu_3(C_6O_6)_2$ in comparison to other topologically similar 2D MOFs that employ larger-sized ligands may be advantageous in producing effective electrical and magnetic modulation due to the condensed molecular binding sites. To minimize the effects resulting from the size and morphological differences of the MOF crystals,[13b] the MOF sample used in the study was prepared using indistinguishable synthetic conditions for the comparison of the electrical and magnetic response triggered by the exposures to the three gases.

Among the three gas molecules we chose, NH_3 and H_2S can both act as Brønsted bases because of the considerable proton affinities on N (854 kJ mol^{-1}) and S atom (705 kJ mol^{-1}) resulting from their electron-rich nature, as shown in the electrostatic potential (ESP) map calculated at 6-311++g level in **Figure 1c**.[19] Bearing lone-pair electrons, both NH_3 and H_2S are also generally classified as electron donors. Their Gutmann's donor numbers (DN), referring to affinity to $SbCl_5$, are much higher than that for water (18 kcal mol^{-1}) entrapped in the pores of the MOFs.[20] Therefore, H_2S and NH_3 can complete with H_2O to bind at Brønsted and Lewis acid sites of the MOF. In addition, H_2S can act as a proton donor and is thus able to interact with basic sites. In contrast, NO is a free radical with an unpaired electron. Nitric oxide can usually combine with other radical species to give closed-shell products or react with transition metals to give metal nitrosyl complexes.[21] Taken together, the reactivity of materials with these probe molecules can provide fundamental insight into the surface chemistry and charge transport of novel materials.

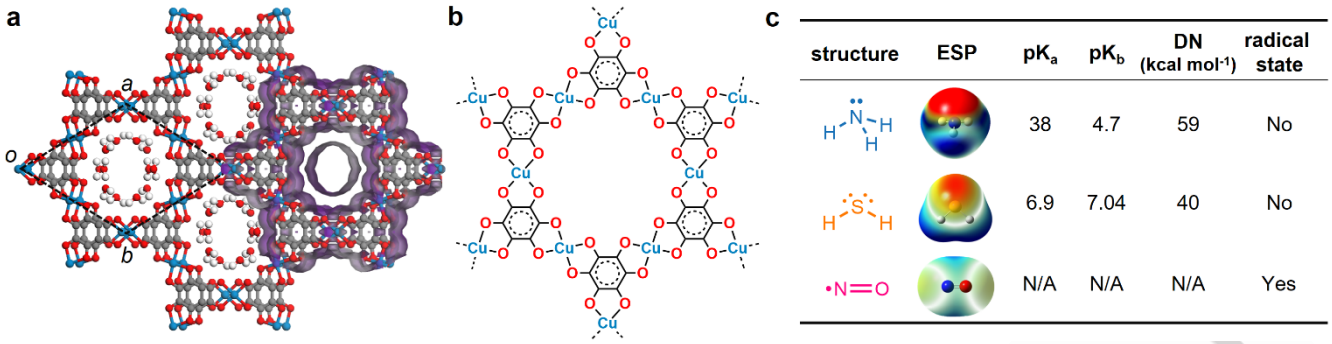

Figure 1. (a) Crystal structure of MOF $Cu_3(C_6O_6)_2$ with accessible pore structure highlighted on the right. (b) Chemical structure of the scaffold of $Cu_3(C_6O_6)_2$. (c) Electronic structures, ESP maps (surface displays with a color gradient of –0.8 to 0.8 eV corresponding to red to blue), and physical and chemical parameters of small gas molecules investigated in this study. The DN number of H_2S is from the value of dimethyl sulfide.

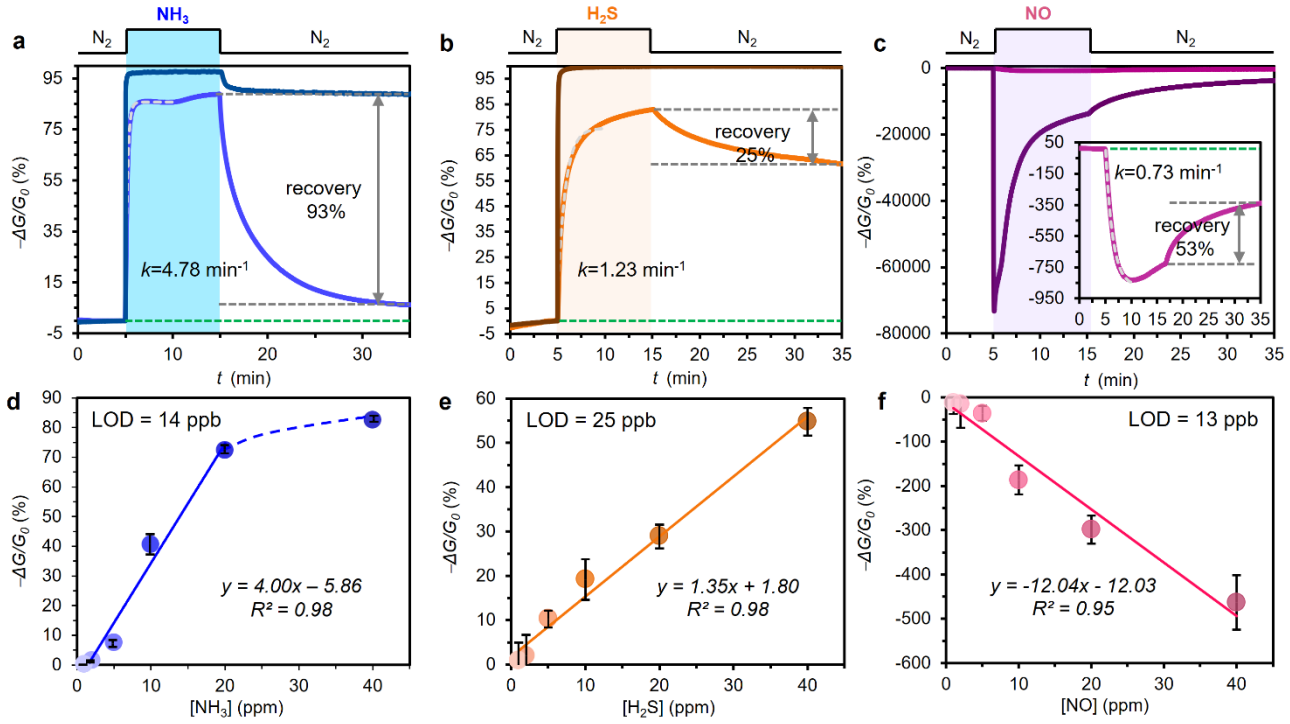

Figure 2. Representative resistance changes of devices made of $Cu_3(C_6O_6)_2$ upon the exposure of 40 ppm and 1% of (a) NH_3, (b) H_2S, and (c) NO. Response curves for 40 ppm and 1% gases are shown with light and dark colors, respectively. The responses of $Cu_3(C_6O_6)_2$ as a function of the concentration of (d) NH_3, (e) H_2S, and (f) NO. The data points represent the average value based on 3-4 replicates and the error bars represent the standard deviation from the average. The response values for NH_3, H_2S, and NO are taken from 1 min exposure, respectively.

Electrical Response

To study the electrical response of the MOF as a function of gas exposure, we fabricated chemiresistive devices by depositing materials on gold interdigitated electrodes. The electrical response of the materials can be estimated using the formula $-\frac{\Delta G}{G_0} = -\frac{I-I_0}{I_0} \times 100\%$, in which I_o and I represent the current of devices during continuous measurement before and after the exposure of the target gases at constant applied voltage. Upon exposure to 40 ppm NH_3, the response of the material reached a plateau within just one minute, with a saturation response of 84.2 ± 1.6%. Notably, this response is among one of the fastest for various reported NH_3 gas sensors at room temperature.[22] Continued NH_3 exposure after 5 min induced a slowly growing response, suggesting the involvement of a new type of interaction that contributes to the electronic perturbation. The response to H_2S was slower than to NH_3. After 10 min of exposure to H_2S, the response increased to 79.4 ± 3.1%, however, a saturation response was not achieved within the tested time range. Compared with NH_3, the response to H_2S was less reversible, only a 25% recovery of the conductance was observed after 20 min N_2 purging. Unlike NH_3 and H_2S, exposure to 40 ppm NO resulted in a negative response of –697.3 ± 42.2% after 10 minutes. The response dropped by 53% after 20 min of recovery in N_2.

To examine the kinetic aspect of the response, we employed a pseudo-first-order kinetic model to analyze the response data at the early stage of the exposure, following established protocols (see Supporting Information for details).[23] The model assumes that the electrical response is proportional to the amount of the analyte adsorbed to the material.[24] The response curves for NH_3 and NO both exhibited a good fit according to the pseudo-first-order kinetic model and yielded rate constants of 4.78 and 0.73 min^{-1}, respectively (**Figures 2a, 2c**). However, the fitting for H_2S only resulted in a moderate fit to this model (**Figure 2b**), suggesting that the observed response to H_2S may involve multiple types of interactions between MOF and H_2S. The rate constant derived from fitting the response curves for H_2S was 1.23 min^{-1}. These distinct rate constants for the three gases may be correlated to the nature of the chemical interactions between the gases and the surface of the MOF, the geometry parameters (size and shape) of the gas molecule, and the availability of binding sites of the gas molecules in MOF $Cu_3(C_6O_6)_2$.

With the exposure of NH_3 and H_2S at a considerably high concentration of 1% (10,000 ppm), the response of the MOF achieved rapid saturation in less than 30 seconds (dark-colored traces in **Figures 2a-b**) with qualitative similarities to the directionality of response, compared to 40 ppm. However, upon exposure to 1% NO, we first observed a large negative response, corresponding to a decrease in resistance, followed by response decay in response intensity during the gas exposure (dark-colored trace in **Figure 2c**). We hypothesized that the initial decrease in resistance could be triggered by NO_2 formed by the oxidation of the NO by the absorbed O_2 molecules within the framework,[25] since NO_2 is known to be a stronger p-type dopant than NO, and the subsequent attenuation of response resulting from consumption of O_2 species. At the high concentration of 1% NO, the response did not follow the pseudo-first-order kinetic model. The use of gas with this high concentration also resulted in much stronger conductivity modifications of the MOF than that under 40 ppm. The corresponding resistance/conductivity changes of the MOF at 1% NH_3, H_2S, and NO were respectively 8, 103, and 25 times higher than that at 40 ppm. The response also was observed to be less reversible for all three gases at 1% than at ppm concentrations.

The $Cu_3(C_6O_6)_2$ MOF showed concentration-dependent responses for the three gases in the tested concentration range of 1–40 ppm (**Figures S2-S4**). Although the responses were distinguishable at 1–40 ppm for NH_3, only a relatively narrow linear range was identified at 1–20 ppm for response values obtained at 10 min exposure (**Figure 2d**). The theoretical limit of detection (LOD) value for NH_3, determined from the response–concentration relationship in the linear range, was found to be 14 ppb. On the other hand, for H_2S and NO, a wider linear range of 1–40 ppm could be identified at a short exposure time of 1 min (**Figures 2e-2f**). The LOD for H_2S and NO were found to be 25 ppb and 13 ppb, respectively. With the prolonged exposure times, the relationship between response values and gas concentrations of H_2S and NO tended toward nonlinear. Long-term reversible cycling test by exposing the MOF devices to 6 sequential exposures of 40 ppm of NH_3, H_2S, and NO showed that the $Cu_3(C_6O_6)_2$ had very good reversibility to the exposure of NH_3 and limited reversibility to the exposure of H_2S and NO (**Figure S9**).

Magnetic Response

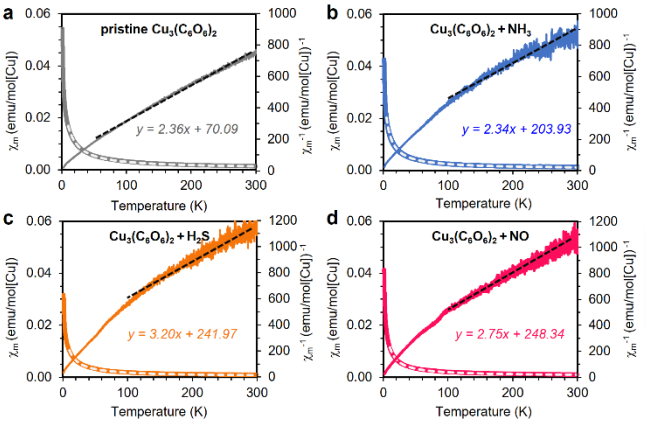

e

materials	Curie constant (C, emu·K·mol^{-1})	Weiss constant (θ, K)	coupling constant (J/k_B, K)
$Cu_3(C_6O_6)_2$	0.42	−30	−27
$Cu_3(C_6O_6)_2$ + NH_3	0.43	−87	−38
$Cu_3(C_6O_6)_2$ + H_2S	0.31	−76	−60
$Cu_3(C_6O_6)_2$ + NO	0.36	−90	−95

Figure 3. FC magnetization for (a) pristine (grey), (b) NH_3 dosed (blue), (c) H_2S dosed (orange), and (d) NO dosed (red) $Cu_3(C_6O_6)_2$ in an applied DC magnetic field of 100 Oe. The white dashed line is the fitting of molar magnetic susceptibility of pristine, NH_3 dosed, H_2S dosed, and NO dosed $Cu_3(C_6O_6)_2$ against the temperature to Curie-Weiss law. (e) Table summarizing the magnetic parameters of the pristine (grey), NH_3 dosed (blue), H_2S dosed (orange), and NO dosed (red) $Cu_3(C_6O_6)_2$. The dosing is for 6 hrs with gas at concentration of 1%.

To examine the magnetic response of the MOF $Cu_3(C_6O_6)_2$ to the three gases, we measured the temperature-dependent magnetic susceptibility of gas-exposed samples (1% gas with duration of exposure of 6 hrs) along with the pristine MOF using a superconducting quantum interference device (SQUID) in the temperature range of 1.8−300 K (**Figure 3a-d**). For all the samples, their field-cooled (FC) and zero-field-cooled (ZFC) magnetization curves were almost indistinguishable in the tested temperature range. The absence of ordering temperature down to 1.8 K suggested a typical paramagnetic behavior at 1.8−300 K for gas exposed samples, which was similar to that found for the pristine MOF. However, after gas exposures, the molar susceptibility decreased compared with that of the pristine MOF. The fitting of magnetic susceptibility χ_m and temperature at 50-300 K according to Curie−Weiss law provided a nearly linear relationship with different slopes for the pristine and gas-exposed samples. The Curie constants were 0.43, 0.31, and 0.36 for the NH_3, H_2S, and NO exposed MOF, respectively. Based on these values, the effective moment (μ_{eff}) calculated for each Cu ion in the formula of $Cu_3(C_6O_6)_2$ was 1.85, 1.57, and 1.70 μ_B, respectively. The μ_{eff} values of H_2S and NO exposed MOF were smaller than that for the pristine MOF (1.83 μ_B), suggesting that the antiferromagnetic interactions between adjacent Cu(II) spins within the layer became stronger after the exposure of H_2S and NO. To estimate the antiferromagnetic coupling interactions, we also analyzed the temperature-dependent χ_m data by high-

temperature series expansion (see Supporting Information for details).[26] The obtained exchange coupling constant for adjacent Cu(II) cations was J/k_B= –38, –60, and –95 K, respectively, for the NH_3, H_2S, and NO exposed MOF. These values again demonstrated that the interaction between the gas molecules and MOF enhanced the antiferromagnetic spin-spin coupling in the MOF.

Spectroscopic Assessment of Material-Analyte Interactions

To investigate the mechanism behind the electrical and magnetic response of $Cu_3(C_6O_6)_2$ caused by the exposure of the gaseous molecules, we first probed the possible structural changes of the MOF caused by gas-MOF interaction by powder X-ray diffraction (pXRD) and micro-crystal electron diffraction (MicroED). pXRD analysis showed that the exposures to the three gases (1% in N_2 for 6 hours) did not alter the intensities of the diffraction peaks of the MOF, suggesting that exposure to these gases did not cause significant changes to the bulk crystallinity of $Cu_3(C_6O_6)_2$ MOF. A closer inspection of the pXRD pattern showed that some of the diffraction peaks shifted in position after gas exposure. Compared with pristine $Cu_3(C_6O_6)_2$, the diffractions of (110) of the MOF after gas exposures all shifted to the higher 2θ positions. Since the (110) is correlated to the in-plane periodicity, the shift of (110) to higher 2θ values indicates a contraction of the MOF channels possibly due to the loss of guest water molecules in the MOF channels. Different from the behavior of the (110) diffraction, the diffraction of a plane $(40\bar{2})$, which is characteristic of the layer-to-layer distance of the MOF, showed gas-dependent behavior. After H_2S exposure, the diffraction of $(40\bar{2})$ shifted to a lower 2θ value, suggesting an expansion of the stacking of the layers induced by the gas. In contrast, NO exposure caused the diffraction of $(40\bar{2})$ to shift to a higher 2θ value, indicating a contraction of layers induced by the gas. No prominent change in the diffraction of $(40\bar{2})$ could be detected after the NH_3 exposure.

To gain additional structural insights, we also examined the gas-exposed samples by micro-crystal electron diffraction. The crystals in the samples exposed to H_2S and NO did not yield diffractions with quality high enough to resolve their structures, which may be due to the disordered nature of the analyte molecules present in the MOF, or the partial structural changes of the MOF that may be undetectable by the general pXRD technique. Fortunately, we were able to resolve the structure of the NH_3 exposed MOF, which shared the same C2/m space group as the pristine MOF (See **Table S5** in Supporting Information). Consistent with the pXRD characterization, the resolved cell parameters of the MOF after NH_3 exposures by MicroED indicated smaller *a* and *b* values compared with those of the pristine MOF. Despite that fact that the exact molecules in the MOF channel were not definitively assigned, the reconstructed 3D potential map showed that the electron density in the MOF channel was significantly reduced compared with the pristine MOF (**Figure 4c-4d**). This observation suggested that the H_2O molecules trapped in the channel of the pristine MOF were likely partially lost after exposure to NH_3.

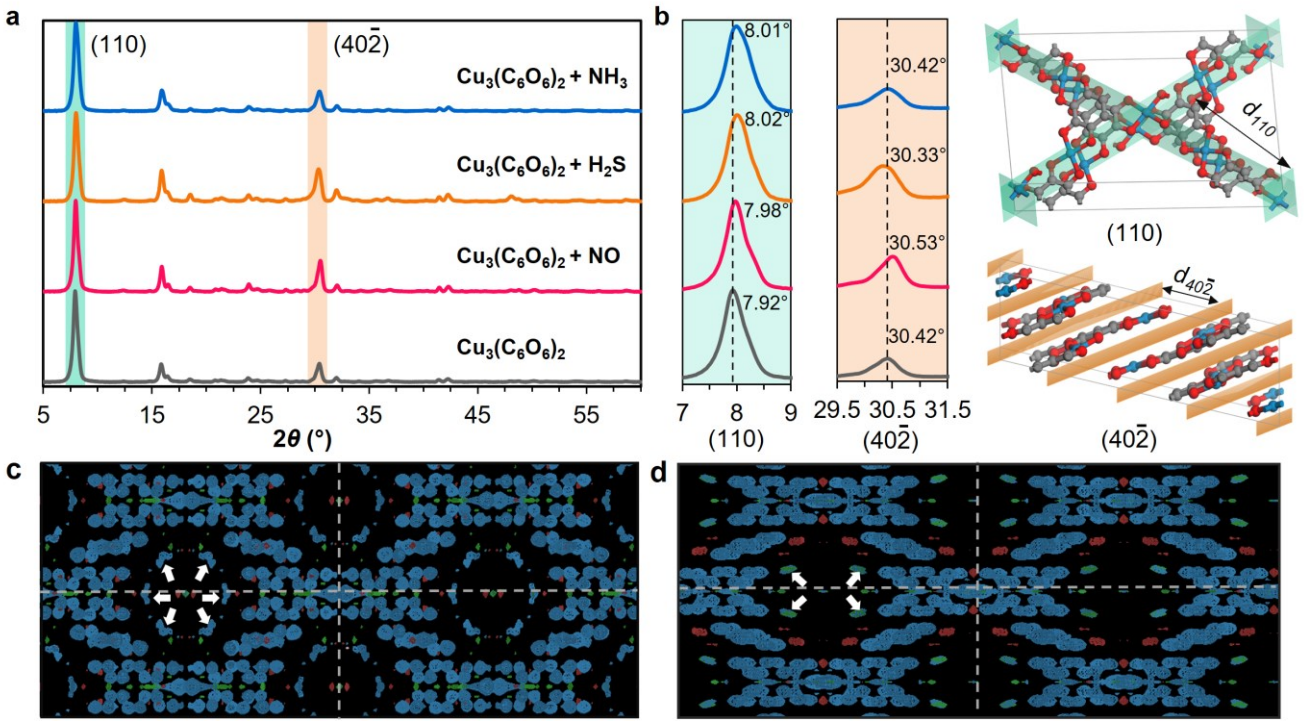

Figure 4. (a) pXRD of the pristine $Cu_3(C_6O_6)_2$ and $Cu_3(C_6O_6)_2$ after exposure to NH_3, H_2S, and NO (1% for 6 hrs). (b) Expanded pXRD and representations for (110) and $(40\bar{2})$. Comparison of the reconstructed 3D potential maps from MicroED data incorporated with the structure model for (c) pristine $Cu_3(C_6O_6)_2$ and (d) NH_3-exposed $Cu_3(C_6O_6)_2$ (viewed along the *c* axis). The white arrows denote the electron density in the pores.

Diffuse reflectance infrared Fourier transform spectroscopy (DRIFTS), X-ray photoelectron spectroscopy (XPS), and electron paramagnetic resonance (EPR) spectroscopy were also used to study the interactions between the MOF and gas molecules. DRIFTS can serve as an in-situ infrared technique to probe material-analyte interactions on surfaces through the intensity

changes or position shifts of characteristic absorption bands.[27] XPS is a surface-sensitive technique and can be used to assess the electronic state change of the compositional elements from the gas-MOF interactions. EPR can determine the presence of species with unpaired spins, which can provide information on the population of unpaired spins caused by changes in the oxidation state of MOF constituents and help identify the immediate magnetic surroundings induced by molecular binding.[28]

As shown in **Figure 5a**, upon continuous exposure to NH_3 (1% in N_2 for 20 min), new adsorption bands at 3319 and 3160 cm^{-1} appeared (marked with dots), which can be ascribed to the stretching modes of NH_3 adsorbed on the material. Compared with the stretching of NH_3 in the gas phase at 3334 cm^{-1} (marked with a star), the relatively small shift indicated that the adsorption of NH_3 on the MOF may be dominated by weak interactions, such as H-bonding with water and coordination with Cu sites. A negatively going band at 3571 cm^{-1} attributed to the stretching modes of water (ν(OH)) was also observed, suggesting that the adsorption of NH_3 molecules by the MOF channels was accompanied by the dehydration process, consistent with the MicroED analysis. The switch of the NH_3 environment to pure N_2 partly restored the spectrum (**Figure S25**), demonstrating that the interaction between NH_3 and $Cu_3(C_6O_6)_2$, including the dehydration process, was partially reversible. After NH_3 exposure, the XPS spectrum of $Cu_3(C_6O_6)_2$ showed a prominent peak at the N 1s range whose intensity is much stronger than the pristine MOF (**Figure 5b**), indicating the uptake of the NH_3 molecules by the MOF. Deconvolution of the N 1s spectrum gave two peaks at 401.2 and 398.6 eV, which can be attributed to NH_3 molecules binding to Brønsted acid site of water ($H_3N{\bullet\bullet\bullet}H_2O$)[29] and Lewis acid site of the Cu ($H_3N{\bullet\bullet\bullet}Cu$),[30] respectively, consistent with the DRIFTS analysis. The EPR spectroscopy of pristine $Cu_3(C_6O_6)_2$ exhibited a broad unsymmetric line shape ascribed to a Cu-centered radical with a pseudo-planar coordination environment.[15, 31] Interestingly, after NH_3 exposure, the EPR signal showed a significantly enhanced unsymmetrical feature accompanied by an intensity increase (**Figure 5c**). These corresponding changes were likely because the binding of NH_3 induced a more anisotropic ligand field of Cu with a possible elongated octahedron configuration[32] and a concomitant charge transfer from Cu to the ligand that shifts the electronic state of Cu, consistent with a previous report.[13b]

The exposure to H_2S caused a significant baseline shift of the spectrum. Since baseline absorbance in region > 1600 cm^{-1} is related to electronic absorption, the significant baseline shift suggested that a strong electronic perturbation was associated with the exposure. Two other prominent changes could also be observed: a new adsorption band at 1003 cm^{-1} which was assigned to the vibration C-OH bond appeared and gradually grew with the prolonged exposure; meanwhile, the broad absorption at around 1425 cm^{-1} from the C-C stretching of the aromatic system went to the negative direction (**Figure 4d**). Furthermore, XPS of H_2S-exposed $Cu_3(C_6O_6)_2$ exhibited a prominent S 2p3/2 peak at the binding energy of 162-165 eV. Deconvolution of the S 2p3/2 spectrum generated three peaks at 161.8, 163.8, and 164.8 eV (**Figure S19**), which we ascribed to Cu_2S, S_x (polysulfide), and CuSH species,[13c, 33] respectively. The possible existence of the Cu_2S and CuSH was consistent with Cu 2p spectrum, where Cu(I) species became the dominant species after H_2S exposure (**Figure 5e**). Taking these clues together, it was hypothesized that, during the exposure to H_2S, the S atom of H_2S attacked the Cu nodes of the MOF and leads to the reduction of Cu(II) to Cu(I). This reduction reaction consequently weakened the coordination bond and resulted in its breakage, regenerating the ligand in the catechol form with the participation of the proton from H_2S. Considering that the bulk crystallinity of the sample after the H_2S exposure largely remains intact, as indicated by pXRD in **Figure 4a**, we inferred that the interaction between the H_2S molecules and the MOF more likely occurs on the surface of the materials instead of in the bulk. The possible irreversible changes to the MOF suggested by XPS and DRIFTS may account for a minor portion of the whole MOF structure, as the elemental analysis suggested that the S: Cu ratio after the H_2S exposure was 1:5.5, much less than 1:1. Nevertheless, the exposure of H_2S significantly increased the unsymmetrical feature of the line shape of the EPR spectrum (**Figure 5f**), corroborating the hypothesized mechanism where the binding of HS^- or S^{2-} likely led to a more anisotropic coordination environment of Cu.[16, 34] The interaction between H_2S and MOF was less reversible compared with that in NH_3 exposure, as the purging with N_2 only brought limited recovery of the spectrum (**Figure S26**).

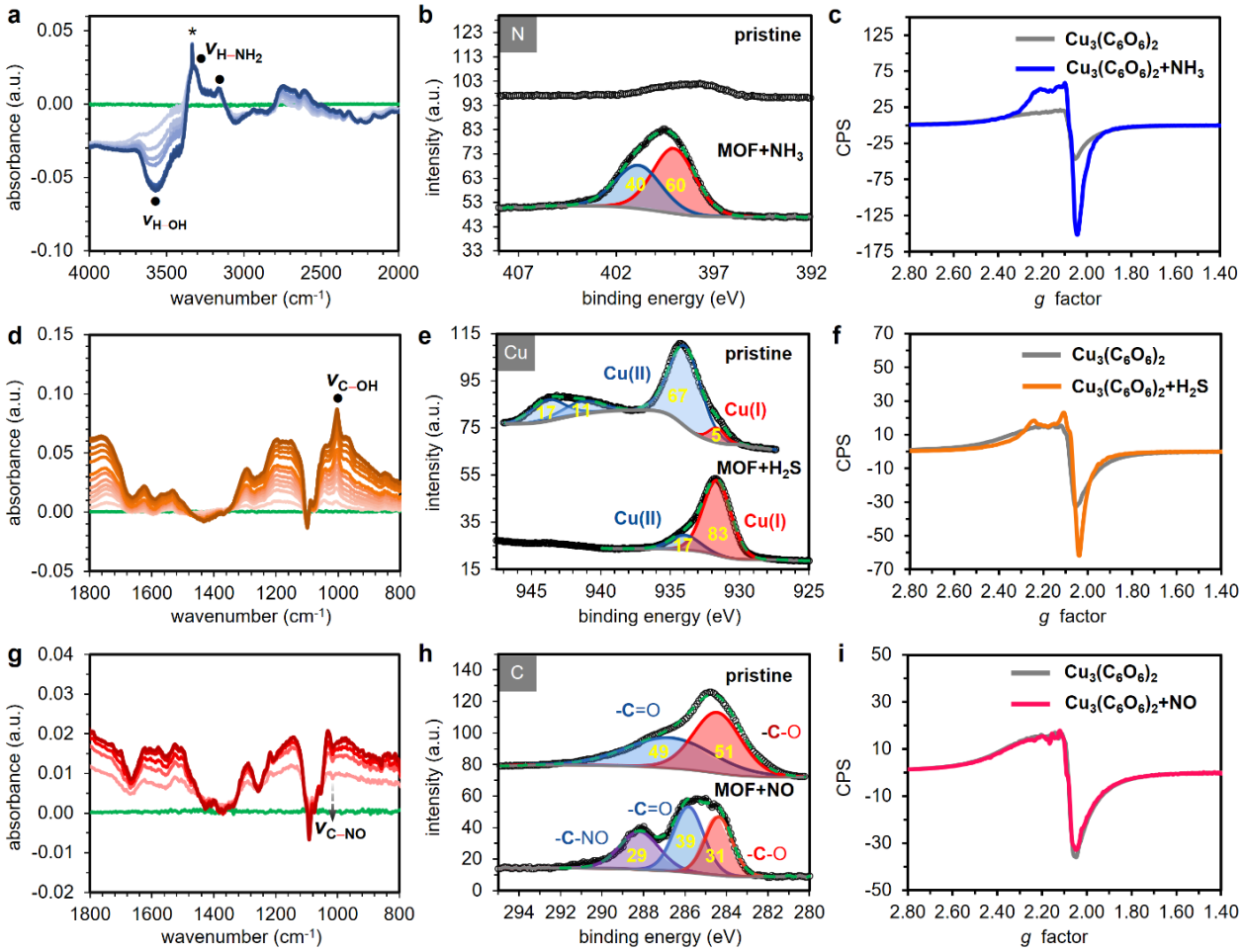

Figure 5. DRIFTS of MOFs after continuous exposure to (a) NH_3, (d) H_2S, and (g) NO (1% in N_2) for 20 min. Comparison of the XPS of the pristine MOF and MOF after 6 hour exposure of (b) NH_3, (e) H_2S, and (h) NO (1% in N_2). Comparison of the EPR of the pristine MOF and MOF at 77 K after 1 hour exposure of (c) NH_3, (f) H_2S, and (i) NO (1% in N_2) of and 10 min N_2 purging.

Exposure to NO also caused a significant baseline shift of the spectrum. In addition to this, a new absorption band at 1033 cm^{-1} emerged after the exposure of NO. This absorption band can be ascribed to C-N stretching (**Figure 5g**), which indicated that NO molecule is likely bound to the carbon atoms of the ligand. As a result, a peak at the binding energy of 288.3 eV appeared in the C 1s XPS spectrum (**Figure S21a**). The much higher binding energy compared to C=O and C-O (**Figure 5h**) suggested the connection of carbon to electron-withdrawing species, consistent with the DRIFTS analysis. The hypothesized interaction can be explained by the fact that NO is a free radical, and that the ligand in $Cu_3(C_6O_6)_2$ is also in a formal –3 radical state ($[C_6O_6]^{3-\bullet}$). Hence, a radical-radical combination would be possible between NO and the ligand of the MOF. Neither the lineshape nor the intensity of the EPR signal showed a significant change after NO exposure (**Figure 5i**), consistent with the Cu 2p XPS spectrum where a similar Cu(II)/Cu(I) ratio to that of the pristine MOF was found after NO exposure (**Figure S21**). These observations support the radical combination mechanism, which mainly involves the radical states of NO and ligand. When each monomer in the ligand dimer binds to a NO molecule, the ligand-NO adduct will remain in a non-radical state. Therefore, we rationalized that the EPR spectrum originating from the Cu-centered radical did not give a significant change after NO exposure.

The above spectroscopic studies provided fundamental insights into the interactions between the three gas molecules and the MOF that induce distinct electrical and magnetic modulation of MOF $Cu_3(C_6O_6)_2$. The spectroscopic data suggest that the interaction between NH_3 and the MOF mostly involves the H-bonding and the coordination of NH_3 to Cu accompanied by the dehydration of the MOF. The reversible nature of the H-bonding and coordination reaction matches the reversibility observed in the chemiresistive response shown in **Figure 2a**. The irreversible dehydration process, which is hypothetically much slower under low concentrations (ppm level) of NH_3 for chemiresistive tests, may be responsible for the slowly-growing response beyond the initial stage of the exposure and the slight irreversibility of the chemiresistive response at ppm-concentrations. The decrease in the conductivity of the MOF $Cu_3(C_6O_6)_2$ induced by NH_3, which is consistent with reported observations in hexahydroxytriphenylene-based MOFs,[13a, 13b, 22] is likely caused by band-gap modulation and doping effect. Spectroscopic investigations confirmed the strong and irreversible interaction between H_2S and the MOF, which likely involved the binding of S atoms to Cu and the subsequent reduction of Cu and partial

breakage of the connection between ligand and Cu. The destructive change of the extended d-π conjugated structure of the MOF can affect the charge transport within the 2D plane. The reduction of Cu in the framework would also reduce the concentration of charge carriers in the p-type semiconductor.[13c] Additionally, the possible formation of polysulfides, which have an insulating effect, may further lead to insulating coatings between MOF crystallites, thereby reducing conductivity.[13c, 33d] This rationale is consistent with the reduced conductivity of the MOF, as observed in the chemiresistive tests. In contrast to the interactions of the MOF with NH_3 and H_2S, we hypothesize that the interaction of NO with the MOF is likely ligand-centered. Considering the higher electronegativity of the N atom in NO, the radical combination of NO and ligand may result in the electron density shifting from the ligand to NO. Thus, this p-type doping of the MOF would lead to a conductivity increase in the MOF, which is consistent with the observed chemiresistive response.[13c, 35]

The characteristic structural changes of the MOFs caused by these MOF-gas interactions also provide the basis for magnetic modulations of the MOFs. In our previous work, we demonstrated that the antiferromagnetic coupling in the MOF is dominated by in-plane Cu(II)-Cu(II) coupling.[15] As demonstrated by Nishihara and coworkers,[36] the electronic states of this type of MOF are associated with a π-d conjugated state, an M-d related state, and a linker state. The observed magnetic modulation could be attributed to the modulation of these states by the electronic interaction between the 2D semi-conductive MOF and the small gas molecules. On one hand, after exposure of the three gases, channel contractions to different degrees occurred to the MOF $Cu_3(C_6O_6)_2$. The shortened in-plane Cu^{II}-Cu^{II} distance in the MOF after gas exposure may be a reason for the enhanced antiferromagnetic spin-spin coupling in the MOF (**Figure 3c**), considering that the strength of antiferromagnetic coupling is reversely correlated to the topological distance.[37] The larger degree of channel contractions after NH_3 and H_2S exposure, as compared to NO exposure, was consistent with the more pronounced enhancements of the antiferromagnetic coupling induced by these analytes. On the other hand, our DFT calculation indicated that in the pristine MOF, where H_2O molecules are hosted within the channels, minor spin densities are found distributed on the oxygen atoms of the H_2O molecules.[15] With the dehydration process upon the NH_3 and H_2S exposure, a redistribution of the spin may occur to promote stronger localization of the radical on the Cu. In addition, the ligand-centered interaction in the case of NO may also enhance the localization of the radical on the Cu. Because antiferromagnetic interaction strength is proportional to the spin populations on the atoms,[38] a higher distribution of spin density on the Cu(II) after gas exposure is expected to enhance the antiferromagnetic coupling.

Conclusion

In this study, we investigated the electrical and magnetic response of a semiconductive, paramagnetic metal–organic framework $Cu_3(C_6O_6)_2$ to small gaseous molecules, NH_3, H_2S, and NO. Chemiresistive tests and magnetic characterizations showed that the MOF displayed changes in electrical conductance and magnetization in response to all three gases. Both NH_3 and H_2S exposure led to the resistance increase of $Cu_3(C_6O_6)_2$ MOF, while NO exposure significantly decreases the resistance. The exposure of the three gases enhanced the magnetic coupling of Cu centers of the MOF and increased the magnetic frustration to different degrees, with NH_3 having the strongest effect followed by H_2S, and then NO. The characteristics of the electrical and magnetic response, including direction, magnitude, or kinetics, are closely dependent on the physicochemical nature of the gaseous molecules. Mechanistic studies through the use of DRIFTS, EPR, and XPS revealed that the underlying molecule-MOF interaction mechanism responsible for the electrical and magnetic response was specific to each gas: NH_3 adsorption was dominated by dehydration, H-bonding, and the coordination of NH_3 to Cu, while H_2S adsorption involved the binding of S atoms to Cu, the possible formation of polysulfide, and the irreversible partial breakage of the connection between ligand and Cu; the binding of NO was characterized by radical type interaction between the NO and the ligand of the MOF.

Our study, for the first time, showed that both the electrical and magnetic responses of a metal–organic framework can be independently correlated to the identity of the analyte molecule. Combining the electronic modulation mechanisms from these two properties—charge and spin of electrons—has the potential to enable the development of highly sensitive and selective electronic devices based on a single responsive material. This work fills a knowledge gap by providing fundamental insights into the effect of material–analyte interaction on the charge and spin modulation of semiconductive and paramagnetic MOFs, especially those with analogous d-π structure to $Cu_3(C_6O_6)_2$. Although the magnetic modulation in the present work results in subtle changes in magnetic exchange interactions, rather than strong on/off spin switching, this work demonstrates the concept of efficient and expedient adsorption of simple gas molecules, not limited to the three types of gas molecules studied here, as a powerful way for the manipulation of electronic properties of this general class of materials. Future work with in-situ studies of magnetic susceptibility and magnetoresistance coupled with the spectroscopic assessment of the MOF would provide further insights into the system regarding the correlation between electrical and magnetic changes upon gas exposure.

Supporting Information

Details for synthetic conditions, chemiresistive tests, magnetic susceptibility measurement, XPS, DRIFTS, and EPR studies are in the supplementary information (PDF).

Acknowledgements

K.A.M. and Z. M. acknowledge support from National Science Foundation EPSCoR award (#1757371), Cottrell Scholar Award (#26019) from the Research Corporation for Science Advancement, NSF CAREER Award (#1945218), Maximizing

Investigators' Research Award from the National Institutes of Health (R35GM138318), and Camille Dreyfus Teacher-Scholar Award. K.A.M. and Z. M. also acknowledge the partial support under PE 0603734A, “Energy and Technology Research in Cold and Arctic Regions,” Task 2 under Contract W913E519C0008 and under PE 0633119, and under Contract W913E520C0010, both managed by the US Army Engineer Research and Development Center (ERDC). H.M.N. would like to acknowledge the Packard Foundation for generous support. C.G.J. would like to acknowledge the National Science Foundation Graduate Research Fellowship Program (DGE-1650604) for funding. This work made use of a Quantum Design MPMS-3 supported by NSF (DMR-1920086) and the Cornell Center for Materials Research Facilities which are supported by the National Science Foundation under Award Number DMR-1719875. The authors thank the University Instrumentation Center at the University of New Hampshire (Durham, NH) for the access to XPS and SEM.

Keywords: electronic modulation • responsive material • metal−organic frameworks • gaseous molecules • chemical sensing

REFERENCES

[1] a) M. A. Stuart, W. T. Huck, J. Genzer, M. Muller, C. Ober, M. Stamm, G. B. Sukhorukov, I. Szleifer, V. V. Tsukruk, M. Urban, F. Winnik, S. Zauscher, I. Luzinov, S. Minko, *Nat. Mater.* **2010**; *9*: 101-113; b) M. Wei, Y. Gao, X. Li, M. J. Serpe, *Polym. Chem.* **2017**; *8*: 127-143; c) M. Mrinalini, S. Prasanthkumar, *Chempluschem* **2019**; *84*: 1103-1121; d) Y. J. Ma, X. Fang, G. Xiao, D. Yan, *Angew. Chem. Int. Ed.* **2021**; *61*; e) B. Zhou, Z. Qi, D. Yan, *Angew. Chem. Int. Ed.* **2022**; *61*: e202208735; f) M. Jeon, M. Kim, J.-S. Lee, H. Kim, S.-J. Choi, H. R. Moon, J. Kim, *ACS Sens.* **2023**; *8*: 3068-3075.

[2] Z. Meng, R. M. Stolz, L. Mendecki, K. A. Mirica, *Chem. Rev.* **2019**; *119*: 478-598.

[3] a) H. Gu, X. Zhang, H. Wei, Y. Huang, S. Wei, Z. Guo, *Chem. Soc. Rev.* **2013**; *42*: 5907-5943; b) J. F. Fennell, Jr., S. F. Liu, J. M. Azzarelli, J. G. Weis, S. Rochat, K. A. Mirica, J. B. Ravnsbaek, T. M. Swager, *Angew. Chem. Int. Ed.* **2016**; *55*: 1266-1281; c) M. J. P. J. W. Orton, Rep. Prog. Phys. 1980, 43, 81-126; d) X. Yang, X. Lin, Y. S. Zhao, D. Yan, *Chem. Eur. J.* **2018**; *24*: 6484-6493.

[4] G. Binasch, P. Grunberg, F. Saurenbach, W. Zinn, *Phys. Rev. B Condens Matter.* **1989**; *39*: 4828-4830.

[5] C. Yang, R. Dong, M. Wang, P. S. Petkov, Z. Zhang, M. Wang, P. Han, M. Ballabio, S. A. Brauninger, Z. Liao, J. Zhang, F. Schwotzer, E. Zschech, H. H. Klauss, E. Canovas, S. Kaskel, M. Bonn, S. Zhou, T. Heine, X. Feng, *Nat. Commun.* **2019**; *10*: 3260.

[6] a) L. E. Darago, M. L. Aubrey, C. J. Yu, M. I. Gonzalez, J. R. Long, *J. Am. Chem. Soc.* **2015**; *137*: 15703-15711; b) R. Jeon le, B. Negru, R. P. Van Duyne, T. D. Harris, *J. Am. Chem. Soc.* **2015**; *137*: 15699-15702; c) J. Zhang, W. Kosaka, Q. Liu, N. Amamizu, Y. Kitagawa, H. Miyasaka, *J. Am. Chem. Soc.* **2023**; *145*: 26179-26189.

[7] a) L. E. Kreno, K. Leong, O. K. Farha, M. Allendorf, R. P. Van Duyne, J. T. Hupp, *Chem. Rev.* **2012**; *112*: 1105-1125; b) H. C. Zhou, J. R. Long, O. M. Yaghi, *Chem. Rev.* **2012**; *112*: 673-674.

[8] M. Ko, L. Mendecki, K. A. Mirica, *Chem. Commun.* **2018**; *54*: 7873-7891.

[9] a) H. Furukawa, K. E. Cordova, M. O'Keeffe, O. M. Yaghi, *Science* **2013**; *341*: 1230444; b) O. M. Yaghi, *J. Am. Chem. Soc.* **2016**; *138*: 15507-15509; c) O. M. Yaghi, M. J. Kalmutzki, C. S. Diercks, *Introduction to Reticular Chemistry*, **2019**; d) L. Sun, M. G. Campbell, M. Dinca, *Angew. Chem. Int. Ed.* **2016**; *55*: 3566-3579; e) E. A. Dolgopolova, O. A. Ejegbavwo, C. R. Martin, M. D. Smith, W. Setyawan, S. G. Karakalos, C. H. Henager, H. C. Zur Loye, N. B. Shustova, *J. Am. Chem. Soc.* **2017**; *139*: 16852-16861.

[10] a) L. S. Xie, G. Skorupskii, M. Dinca, *Chem. Rev.* **2020**; *120*: 8536-8580; b) L. Sun, M. G. Campbell, M. Dincă, *Angew. Chem. Int. Ed.* **2016**; *55*: 3566-3579.

[11] a) G. Minguez Espallargas, E. Coronado, *Chem. Soc. Rev.* **2018**; *47*: 533-557; b) A. E. Thorarinsdottir, T. D. Harris, *Chem. Rev.* **2020**; *120*: 8716-8789.

[12] a) J. G. Calvert, A. Lazrus, G. L. Kok, B. G. Heikes, J. G. Walega, J. Lind, C. A. Cantrell, *Nature* **1985**; *317*: 27-35; b) R. Kant, S. Bhattacharya, in *Environmental, Chemical and Medical Sensors*, **2018**, pp. 9-30; c) A. K. Mustafa, M. M. Gadalla, S. H. Snyder, *Sci. Signal.* **2009**; *2*: re2; d) S. Edelson, *Science-Business eXchange* **2010**; *3*: 578-578; e) M. A. Singer, *Med. Hypotheses* **2001**; *57*: 740-744.

[13] a) V. Rubio-Gimenez, N. Almora-Barrios, G. Escorcia-Ariza, M. Galbiati, M. Sessolo, S. Tatay, C. Marti-Gastaldo, *Angew. Chem. Int. Ed.* **2018**; *57*: 15086-15090; b) R. M. Stolz, A. Mahdavi-Shakib, B. G. Frederick, K. A. Mirica, *Chem. Mater.* **2020**; *32*: 7639-7652; c) A. M. Eagleton, M. Ko, R. M. Stolz, N. Vereshchuk, Z. Meng, L. Mendecki, A. M. Levenson, C. Huang, K. C. MacVeagh, A. Mahdavi-Shakib, J. J. Mahle, G. W. Peterson, B. G. Frederick, K. A. Mirica, *J. Am. Chem. Soc.* **2022**; *144*: 23297-23312.

[14] a) J. Park, A. C. Hinckley, Z. Huang, D. Feng, A. A. Yakovenko, M. Lee, S. Chen, X. Zou, Z. Bao, *J. Am. Chem. Soc.* **2018**; *140*: 14533-14537; b) M. Choe, J. Y. Koo, I. Park, H. Ohtsu, J. H. Shim, H. C. Choi, S. S. Park, *J. Am. Chem. Soc.* **2022**; *144*: 16726-16731.

[15] Z. Meng, C. G. Jones, S. Farid, I. U. Khan, H. M. Nelson, K. A. Mirica, *Angew. Chem. Int. Ed.* **2022**; *61*: e202113569.

[16] Q. Chen, O. Adeniran, Z. F. Liu, Z. Zhang, K. Awaga, *J. Am. Chem. Soc.* **2023**; *145*: 1062-1071.

[17] a) M. Hmadeh, Z. Lu, Z. Liu, F. Gándara, H. Furukawa, S. Wan, V. Augustyn, R. Chang, L. Liao, F. Zhou, E. Perre, V. Ozolins, K. Suenaga, X. Duan, B. Dunn, Y. Yamamto, O. Terasaki, O. M. Yaghi, *Chem. Mater.* **2012**; *24*: 3511-3513; b) J.-H. Dou, M. Q. Arguilla, Y. Luo, J. Li, W. Zhang, L. Sun, J. L. Mancuso, L. Yang, T. Chen, L. R. Parent, G. Skorupskii, N. J. Libretto, C. Sun, M. C. Yang, P. V. Dip, E. J. Brignole, J. T. Miller, J. Kong, C. H. Hendon, J. Sun, M. Dincă, *Nat. Mater.* **2020**; *20*: 222-228.

[18] S. Kang, M. Jeon, J. Kim, *ACS Sens.* **2023**; *8*: 3448-3457.

[19] R. Yamdagni, P. Kebarle, *J. Am. Chem. Soc.* **2002**; *98*: 1320-1324.

[20] F. Cataldo, *Eur. Chem. Bull.* **2015**; *4*: 92-97.

[21] P. C. Ford, J. C. M. Pereira, K. M. Miranda, in *Nitrosyl Complexes in Inorganic Chemistry, Biochemistry and Medicine II*, **2013**, pp. 99-135.

[22] M. S. Yao, X. J. Lv, Z. H. Fu, W. H. Li, W. H. Deng, G. D. Wu, G. Xu, *Angew. Chem. Int. Ed.* **2017**; *56*: 16510-16514.

[23] F. I. Bohrer, A. Sharoni, C. Colesniuc, J. Park, I. K. Schuller, A. C. Kummel, W. C. Trogler, *J. Am. Chem. Soc.* **2007**; *129*: 5640-5646.

[24] J. Kong, A. Javey, *Carbon Nanotube Electronics*, **2009**.

[25] V. P. Verma, S. Das, S. Hwang, H. Choi, M. Jeon, W. Choi, *Materials Science and Engineering: B* **2010**; *171*: 45-49.

[26] J. Oitmaa, C. Hamer, W. Zheng, *Series Expansion Methods for Strongly Interacting Lattice Models*, **2010**.

[27] M. B. Mitchell, in *Structure-Property Relations in Polymers*, **1993**, pp. 351-375.

[28] M. Chiesa, E. Giamello, M. Che, *Chem. Rev.* **2010**; *110*: 1320-1347.

[29] Y. Ma, W. Lu, X. Han, Y. Chen, I. da Silva, D. Lee, A. M. Sheveleva, Z. Wang, J. Li, W. Li, M. Fan, S. Xu, F. Tuna, E. J. L. McInnes, Y. Cheng, S. Rudic, P. Manuel, M. D. Frogley, A. J. Ramirez-Cuesta, M. Schroder, S. Yang, *J. Am. Chem. Soc.* **2022**; *144*: 8624-8632.

[30] A. Galtayries, E. Laksono, J. M. Siffre, C. Argile, P. Marcus, *Surf. Interface Anal.* **2000**; *30*: 140-144.

[31] B. Kozlevcar, P. Segedin, *Croat Chem Acta* **2008**; *81*: 369-379.

[32] E. Garribba, G. Micera, *J. Chem. Educ.* **2006**; *83*.

[33] a) A. Galtayries, J. P. Bonnelle, *Surf. Interface Anal.* **2004**; *23*: 171-179; b) M. Fantauzzi, B. Elsener, D. Atzei, A. Rigoldi, A. Rossi, *RSC Adv.* **2015**; *5*: 75953-75963; c) E. Martínez-Ahumada, A. López-Olvera, V. Jancik, J. E. Sánchez-Bautista, E. González-Zamora, V. Martis, D. R. Williams, I. A. Ibarra, *Organometallics* **2020**; *39*: 883-915; d) A. López-Olvera, J. G. Flores, J. Aguilar-Pliego, C. K. Brozek, A. Gutiérrez-Alejandre, I. A. Ibarra, *Chem. Mater.* **2021**; *33*: 6269-6276.

[34] a) P. Basu, *J. Chem. Educ.* **2001**; *78*; b) S. Ye, *Magn. Reson. Lett.* **2023**; *3*: 43-60.

[35] a) M. K. Smith, K. E. Jensen, P. A. Pivak, K. A. Mirica, *Chem. Mater.* **2016**; *28*: 5264-5268; b) A.-Q. Wu, W.-Q. Wang, H.-B. Zhan, L.-A. Cao, X.-L. Ye, J.-J. Zheng, P. N. Kumar, K. Chiranjeevulu, W.-H. Deng, G.-E. Wang, M.-S. Yao, G. Xu, *Nano Res.* **2020**; *14*: 438-443.

[36] K. Sakaushi, H. Nishihara, *Acc Chem Res* **2021**; *54*: 3003-3015.

[37] R. Wang, C. H. Ko, A. M. Brugh, Y. Bai, M. D. E. Forbes, M. J. Therien, *J. Phys. Chem. A* **2020**; *124*: 7411-7415.

[38] H. M. McConnell, *J. Chem. Phys.* **1963**; *39*: 1910-1910.

Entry for the Table of Contents

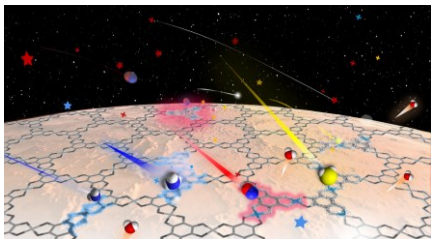

Exposure to gaseous molecules can induce characteristic electrical and magnetic property changes of a semiconductive metal-organic framework (MOF). The underlying interaction mechanism responsible for the electrical and magnetic modulation is found related to the intrinsic physical and chemical properties of the participating molecules which cause specific electronic and structural changes of the MOF.

Institute and/or researcher Twitter usernames: Katherine Mirica@KMirica; Nelson Group@TheNelsonLab